



## ORIGINAL ARTICLE

# Synthesis of $\text{NaKCO}_3@(\text{Mn-Na}_2\text{WO}_4/\text{SiO}_2)$ core-shell catalyst for oxidative coupling of methane



Hadis Rezaee<sup>a</sup>, Mir Esmaeil Masoumi<sup>a,\*</sup>, Afshar Alihosseini<sup>b</sup>

<sup>a</sup> Department of Chemical Engineering, North Tehran Branch, Islamic Azad University, Tehran, Iran

<sup>b</sup> Department of Chemical Engineering, Central Tehran Branch, Islamic Azad University, Tehran, Iran

Received 24 September 2022; accepted 13 January 2023

Available online 20 January 2023

## KEYWORDS

Oxidative Coupling of Methane;  
Ethylene;  
Nano-catalyst;  
Core-shell;  
Shell

**Abstract** Oxidative Coupling of Methane (OCM) is a process to produce ethylene as one of the most widely used petrochemicals from methane natural gas. The core-shell nano-catalyst of  $\text{NaKCO}_3@(\text{Mn} - \text{Na}_2\text{WO}_4/\text{SiO}_2)$  was prepared with different ratios of Na/K, and its activity in the OCM process was investigated and its performance was compared with the conventional  $\text{Mn} - \text{Na}_2\text{WO}_4/\text{SiO}_2$  nano-catalyst. The effect of temperature and methane-to-oxygen ratio on nano-catalyst performance was investigated. The performance criteria included methane conversion, ethylene selectivity, and  $\text{C}_2^+$  yield. The formation of the core-shell structure has been deliberated using XRD and FE-SEM characterization tests. The results of characterization and reactor experiments indicated that the best performance was related to the nano-catalyst prepared with a ratio of  $\text{Na/K} = 2/2.4$ , operating conditions: 850 °C, atmospheric pressure, and  $\text{CH}_4/\text{O}_2$  ratio = 2 in the reaction feed. The formation of the core-shell structure does not reduce the nano-catalyst activity, but rather increases the selectivity of the main product, ethylene, by improving the nano-catalyst performance even at 850 °C. Stability tests were performed to examine the catalytic activity under high temperatures.

© 2023 The Author(s). Published by Elsevier B.V. on behalf of King Saud University. This is an open access article under the CC BY-NC-ND license (<http://creativecommons.org/licenses/by-nc-nd/4.0/>).

## 1. Introduction

Ethylene is an important chemical compound and is used in the synthesis of the chain products in the petrochemical industry which include raw materials as polyethylene, polypropylene, and polystyrene, which are used in the production of a wide range of products from car anti-freeze to plastics (Zhang et al., 2021a). Therefore, ethylene is categorized as a first-class hydrocarbon in the chemical and petrochemical industry. Over the past 30 years, studies have been made in ethylene production by OCM. The reaction mechanism of the catalysts in the OCM process is as follows (Raza et al., 2022):

\* Corresponding author.

E-mail address: [m\\_masoumi@iau-tnb.ac.ir](mailto:m_masoumi@iau-tnb.ac.ir) (M.E. Masoumi).

Peer review under responsibility of King Saud University.



Production and hosting by Elsevier



The OCM process shows promise in  $\text{CH}_4$  conversion to  $\text{C}_2\text{H}_4$  and  $\text{C}_2\text{H}_6$  hence, accounting for a succinct approach to use natural gas for ethylene production as the OCM technique applies direct conversion making it possible to avoid the synthesis gas step (Lee et al., 2022).

The catalyst that is used in the OCM process is vital as it affects the ethylene selectivity and methane conversion percentage. The oxide catalysts are the foremost catalysts used in the OCM reactions. These catalysts can be either, the modified oxides of the transition metals or the promoted or the assorted ones of group IA and IIA elements (Wang et al., 2016).

It has been identified that the  $\text{Mn} - \text{Na}_2\text{WO}_4/\text{SiO}_2$  catalyst has performed more efficiently, amid all the catalysts synthesized for the OCM process as its stability is high for long duration on the reaction stream. The emerging wetness impregnation technique is the most appropriate synthesis method among the existing methods (Jafarzadeh et al., 2022) to synthesize the  $\text{Na}_2\text{WO}_4/\text{SiO}_2$  catalyst.

The active components (Mn, Na, and W) on or close to the surface of the catalyst are enriched by this process. This could cause a damage of dynamic constituent through lengthy periods on stream which eventually brings about improved catalyst enactment. A distinction of the composition was exactly premeditated (J. Zhang et al., 2021) and it was observed that on protecting the content of Mn stable at 2 % wt. and changing the content of  $\text{Na}_2\text{WO}_4$ , the supreme activity of OCM was achieved at 5 % wt. of  $\text{Na}_2\text{WO}_4$ . It has been suggested that  $\text{Na}_2\text{WO}_4$  and Mn serve as active component and promoters, consistently (Ortiz-Bravo et al., 2021) although the reaction mechanism is still controversial. Researchers have added supporters and changed the support to improve the  $\text{Mn} - \text{Na}_2\text{WO}_4/\text{SiO}_2$  catalyst (Zhang et al., 2022). Since the OCM reaction is active at very high temperatures, one of the ways to protect the catalyst, the active phase, and the product at the same time is to form a core-shell structure for the catalyst; so, the active phase is selected as the core (Alli et al., 2022).

In the last two decades, OCM research has mainly focused on the synthesis of suitable catalysts and the evaluation of reaction mechanisms to achieve formulations with acceptable outcomes (X. Gao et al., 2022). The main goal of all research in this field is to attain a high ethylene selectivity and acceptable methane conversion percentage, in one step through the catalytic system. Since the 1990 s, major research has focused on optimizing catalysts and examining the types of OCM reactors, in addition to catalyst formulation, selectivity and deactivation of a catalyst in due course is very important (Lyu et al., 2022).

Jaroenpanon et al. (Jaroenpanon et al., 2022) studied the performance of  $\text{Na}_2\text{WO}_4 - \text{Mn}_x\text{O}_y$  on  $\text{SiO}_2$  or  $\text{La}_2\text{O}_3$  catalysts in powder and fiber form for OCM reaction. Their results showed that fiber catalysts increase  $\text{CH}_4$  conversion and  $\text{C}_2^+$  selectivity due to improved heat and mass diffusion in the catalyst bed. The activation of  $\text{CH}_4$  at low temperature is strongly associated with the presence of oxygen species at a relatively lower binding energy, which allows the oxygen species to be readily allocated during the reaction. Nevertheless, the  $\text{C}_2^+$  efficiency of NWMSi catalysts, especially for NWMSi - F, was reported to be higher than that of NWMLa under the same conditions, due to the synergistic catalytic effect of the active phases, including  $\text{Na}_2\text{WO}_4$ ,  $\text{Mn}_x - \text{O}_y$ , and  $\alpha - \text{cristobalite}$ .

Tiyatha et al. (Tiyatha et al., 2022) for  $\text{MnTiO}_3 - \text{Na}_2\text{WO}_4$  and  $\text{MnO}_x - \text{TiO}_2 - \text{Na}_2\text{WO}_4$  catalysts, the effect of loading  $\text{MnTiO}_3$  or  $\text{MnO}_x - \text{TiO}_2$ , respectively, on two different supports  $\text{SiO}_2\text{S}$  sol-gel (SG) and commercial carbonated  $\text{SiO}_2$  (CS) studied. Their results showed that the catalyst with the highest  $\text{C}_2^+$  efficiency (21.6 % with 60.8 %  $\text{C}_2^+$  selectivity and 35.6 %  $\text{CH}_4$  conversion) was 10 wt%

$\text{MnTiO}_3 - \text{Na}_2\text{WO}_4/\text{SG}$  with an olefin/paraffin ratio of 2.2. Also, stability tests for more than 24 h showed that SG-supported catalysts were more durable than those on CS, because the active phase (especially  $\text{Na}_2\text{WO}_4$ ) was more stable on SG than on CS.

Reportedly, a perfect connection amid the enactment and under the conditions of OCM, the conductivity was detected, and the highest electrical conductivity was scored by Mn (Yentekakis et al., 2021). Although  $\alpha$ -cristobalite has been detected in these catalysts composed of other dissimilar elements, W presented the greatest  $\text{C}_2$  selectivity and greatest  $\text{CH}_4$  conversion over the rest and phase transfer from amorphous  $\text{SiO}_2$  (Orooji et al., 2022). A study of different support materials was carried out and concluded that  $\text{SiO}_2$  was the best support for the Mn -  $\text{Na}_2\text{WO}_4$  (Song et al., 2022).

Gärtner et al. (Gärtner et al., 2014) used core-shell catalysts to produce ethylene in the oxidative dehydrogenation of ethane. The support of the  $\text{LiKCl}/\text{MgO}/\text{Dy}_2\text{O}_3$  catalyst was solid and coated by a LiKCl shell; during the shell process, the active oxygen species diffuse through the molten chloride shell and convert to  $\text{O}^-$  and, react with ethane on the surface of the shell, the final product is ethylene and water. In similar research, they succeeded to achieve 95 % selectivity with a 25 % conversion percentage by oxidation in the molten shell of this catalyst with an overlayer of 40 % molar; the higher molar percentage of its overlayer corresponds to a lower conversion percentage and higher ethylene selectivity. The best overlayer percentage was 40 % (Liu et al., 2022). In this study, we scrutinize the activity and stability of  $\text{NaKCO}_3@(\text{Mn} - \text{Na}_2\text{WO}_4/\text{SiO}_2)$  as core-shell catalyst and compare it with conventional active/base phase Mn -  $\text{Na}_2\text{WO}_4/\text{SiO}_2$  catalyst in the OCM process. The temperature and methane to oxygen ratio have been selected as parameters to investigate the behavior of both catalysts. For core-shell catalyst, in addition to the above two variables, the effect of Na/K ratio and for base/active phase catalyst, the effect of Mn/ $\text{Na}_2\text{WO}_4$  ratio have also been investigated.

## 2. Experimental

### 2.1. Materials

The amorphous  $\text{SiO}_2$  (35/60 mesh size, Davisil grade 646), manganese (II) nitrate hexahydrate ( $\text{Mn}(\text{NO}_3)_2 \cdot 6\text{H}_2\text{O}$ ), sodium tungstate (VI) dehydrate ( $\text{Na}_2\text{WO}_4 \cdot 2\text{H}_2\text{O}$ ), potassium carbonate ( $\text{K}_2\text{CO}_3$ ) and sodium carbonate ( $\text{Na}_2\text{CO}_3$ ) were purchased from *Sigma-Aldrich*.

### 2.2. Preparation of Mn - $\text{Na}_2\text{WO}_4/\text{SiO}_2$

The amorphous  $\text{SiO}_2$  was used as support for all samples. An aqueous solution comprising an 50 ml of  $\text{Mn}(\text{NO}_3)_2 \cdot 4\text{H}_2\text{O}$  (20 M) was prepared by impregnating a 20 g of silica gel ( $\text{SiO}_2$ ) particles. The granules were air-dried at a temperature of 130 °C for 5 h. Then 50 ml of 10 M  $\text{Na}_2\text{WO}_4 \cdot 2\text{H}_2\text{O}$  solution was added to the granules. Next, the samples were dehydrated for 8 h at 130 °C. The end, all samples was calcined at 800 °C (Ortiz-Bravo et al., 2021), for 8 h with the heating rate set at 10 °C  $\text{min}^{-1}$  (Table 1).

**Table 1** Prepared catalysts.

Name	Sample
2Mn - 4 $\text{Na}_2\text{WO}_4/\text{SiO}_2$	AS-1
2Mn - 5 $\text{Na}_2\text{WO}_4/\text{SiO}_2$	AS-2
2Mn - 6 $\text{Na}_2\text{WO}_4/\text{SiO}_2$	AS-3
$\text{NaKCO}_3@(\text{Mn} - \text{Na}_2\text{WO}_4/\text{SiO}_2)(\text{Na}/\text{K} = 1/1.2)$	CS-1
$\text{NaKCO}_3@(\text{Mn} - \text{Na}_2\text{WO}_4/\text{SiO}_2)(\text{Na}/\text{K} = 2/2.4)$	CS-2
$\text{NaKCO}_3@(\text{Mn} - \text{Na}_2\text{WO}_4/\text{SiO}_2)(\text{Na}/\text{K} = 3/3.6)$	CS-3

### 2.3. Preparation of $\text{NaKCO}_3@(\text{Mn}-\text{Na}_2\text{WO}_4/\text{SiO}_2)$ core-shell structures

The core-shell catalyst  $\text{NaKCO}_3@(\text{Mn}-\text{Na}_2\text{WO}_4/\text{SiO}_2)$  was synthesized by combining different percentages of K and Na using wet impregnation method.  $2\text{Mn}-5\text{Na}_2\text{WO}_4/\text{SiO}_2$  was used as the core for this catalyst with the new method. Certain amount of  $\text{Mn}-\text{Na}_2\text{WO}_4/\text{SiO}_2$  was slowly added to a 250 ml deionized water containing 50 ml of  $\text{Na}_2\text{CO}_3$  solution while being stirred at 500 rpm at 80 °C. After complete dissolution of the material, it was placed in an oven at 100 °C for 12 h until water evaporated and, a porous solid remained. The dried solid was separated and powdered. Then, it was added to a

250 ml solution containing the second layer including an aqueous solution of  $\text{K}_2\text{CO}_3$ , similar to the previous step. The mixture was placed in an oven at 100 °C for 12 h and after complete drying, for the calcination step and removal of excess material from the catalyst structure, the resulting powder was placed in a furnace and exposed to a flow of synthetic air gas at a temperature of 800 °C (Ortiz-Bravo et al., 2021) with a ramp of 10 °C  $\text{min}^{-1}$  for 8 h (Table 1).

### 2.4. Characterization of catalyst

The crystal constructions of the arranged catalysts were established through measuring the powder X-ray diffraction (XRD)

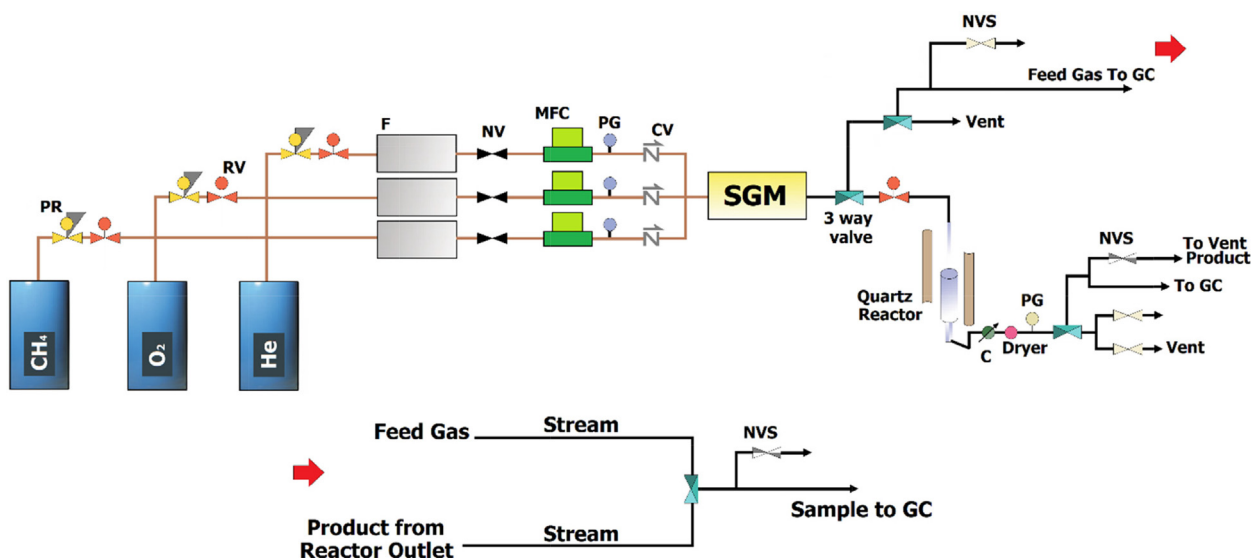


Fig. 1 Schematic Design of the OCM Process.

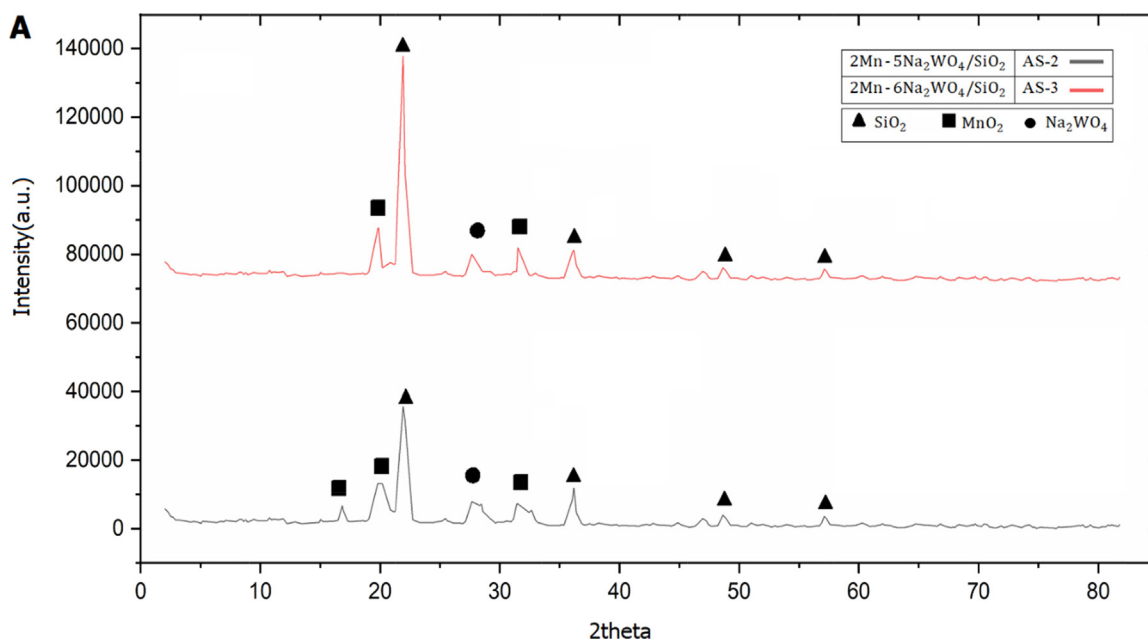


Fig. 2 XRD patterns of catalysts samples: a) AS-2 and AS-3, b) CS-1 and CS-2, and c) CS-3 and AS-1.

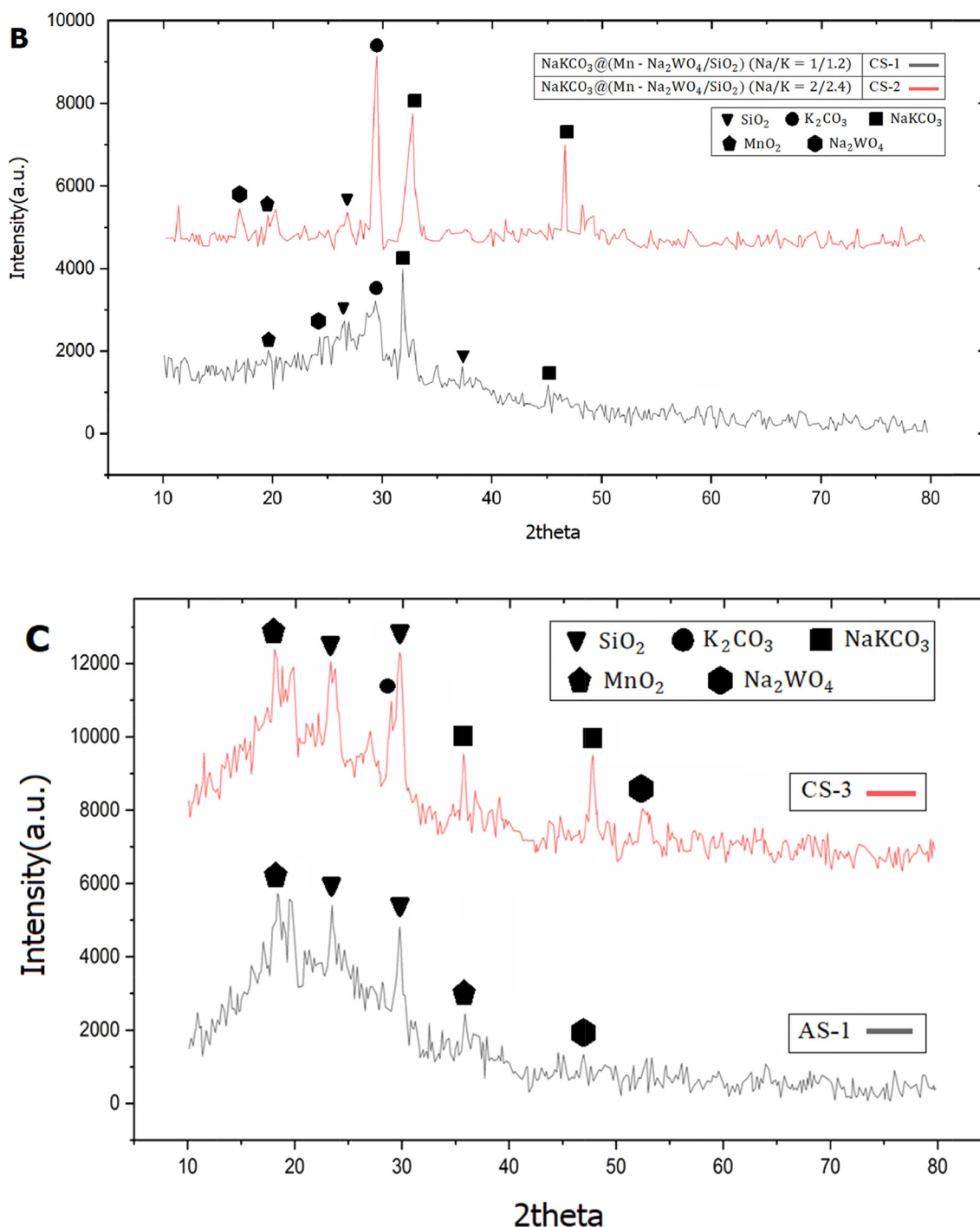
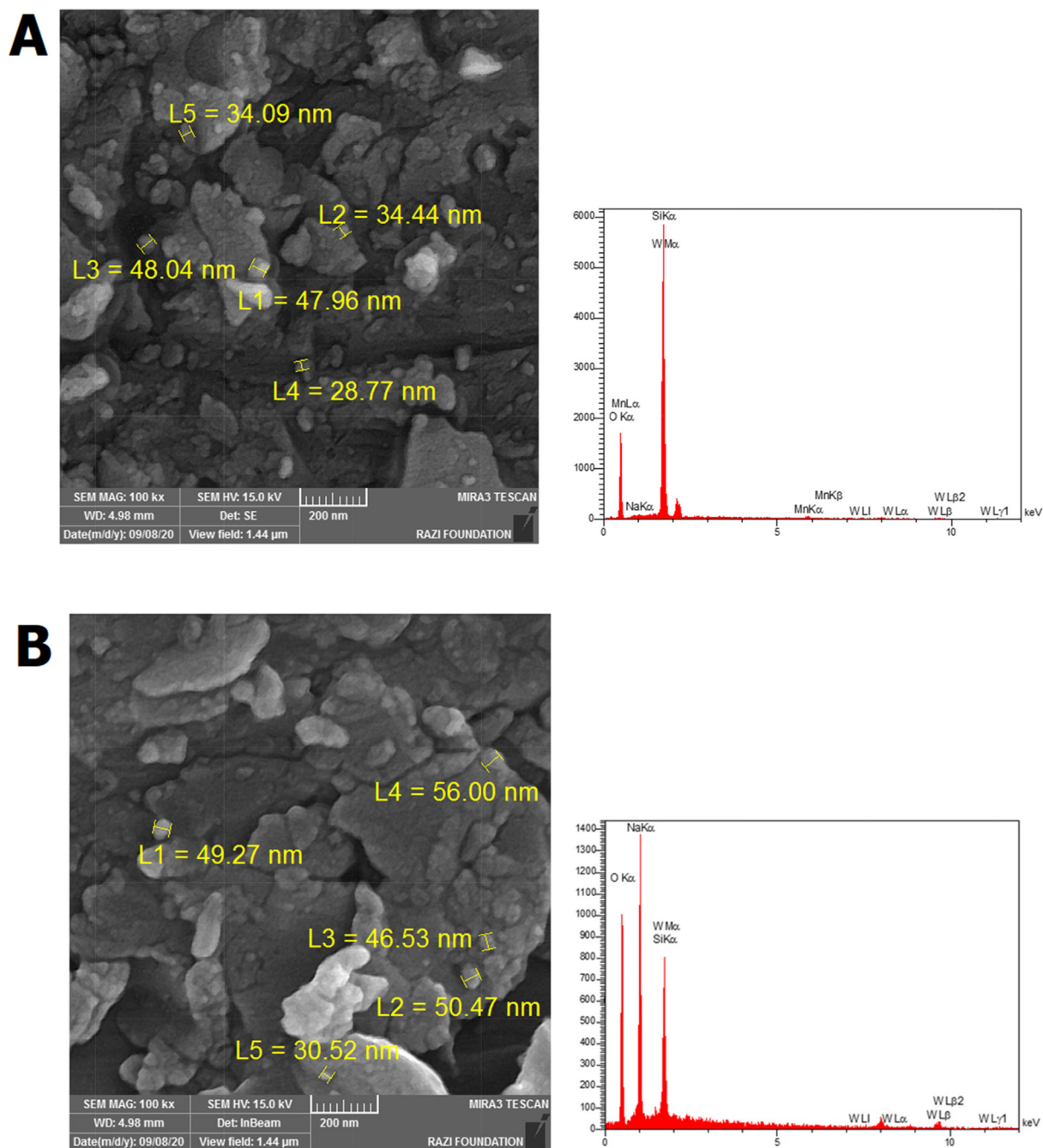


Fig. 2 (continued)

**Table 2** BET surface area and pore-volume of catalysts.

Catalysts	BET Surface area ( $\text{m}^2\text{g}^{-1}$ )	Pore-volume ( $\text{cm}^3\text{g}^{-1}$ )
AS-1	68.26	0.75
AS-2	50.25	0.8
AS-3	43.12	0.9
CS-1	48.56	0.02
CS-2	89.25	0.91
CS-3	78.36	0.74

through an X'pert-Pro diffractometer (Philips, Model: PW1730, Netherlands) by  $\text{Cu K}\alpha$  radiation (Step size = 0.05 deg, Time Per Step = 1 s, Wavelength of copper X-ray lamp = 1.54056 Å., Voltage = 40 kV, Current = 30 mA, Software XPert HighScore Plus v3.0e). The BET test was carried out with Quanta chrome Chem BET 3000 instruments, for measuring the surface area (The temperature of liquid nitrogen 77 K, Dehydration temperature of 120 °C for 2 h). A scanning electron microscope with an energy dispersive X-ray spectrom-



**Fig. 3** FE-SEM images and EDX graphs for all samples AS-2 (a), AS-3 (b), CS-1 (c), and CS-2 (d).

eter (FE-SEM/EDS, Tescan, Czech) was used to image the surface morphology of the catalysts. Transmission electron microscope (TEM, HT7800 Hitachi, Japan) was used to investigate the core-shell structure of catalysts. Thermal Gravimetric Analysis test was performed using PL-TGA device for measuring the amount of carbon deposition on the catalysts.

### 2.5. Catalyst activity and stability

In order to perform the activity test, the reactor temperature and pressure were fixed at 850 °C and 1 atm, respectively. A

quartz tube reactor with an inner diameter of 5 mm at atmospheric pressure was applied to measure the catalytic activity in the OCM reaction. (1) g of synthesized catalysts were diluted by 3 g sieved quartz powder (30/60 mesh size). The bed of the catalyst was placed at the midpoint of the reactor. To avoid the catalyst from spilling to the base of the reactor, the mixture of catalyst and quartz was poured into the quartz reactor. To mix and preheat the gases, some quartz powder was present on top of the catalyst. For the next step, the reactor was placed inside a furnace and gas transmission lines were joined.  $\text{N}_2$  was applied to dilute the  $\text{CH}_4$  and  $\text{O}_2$  with

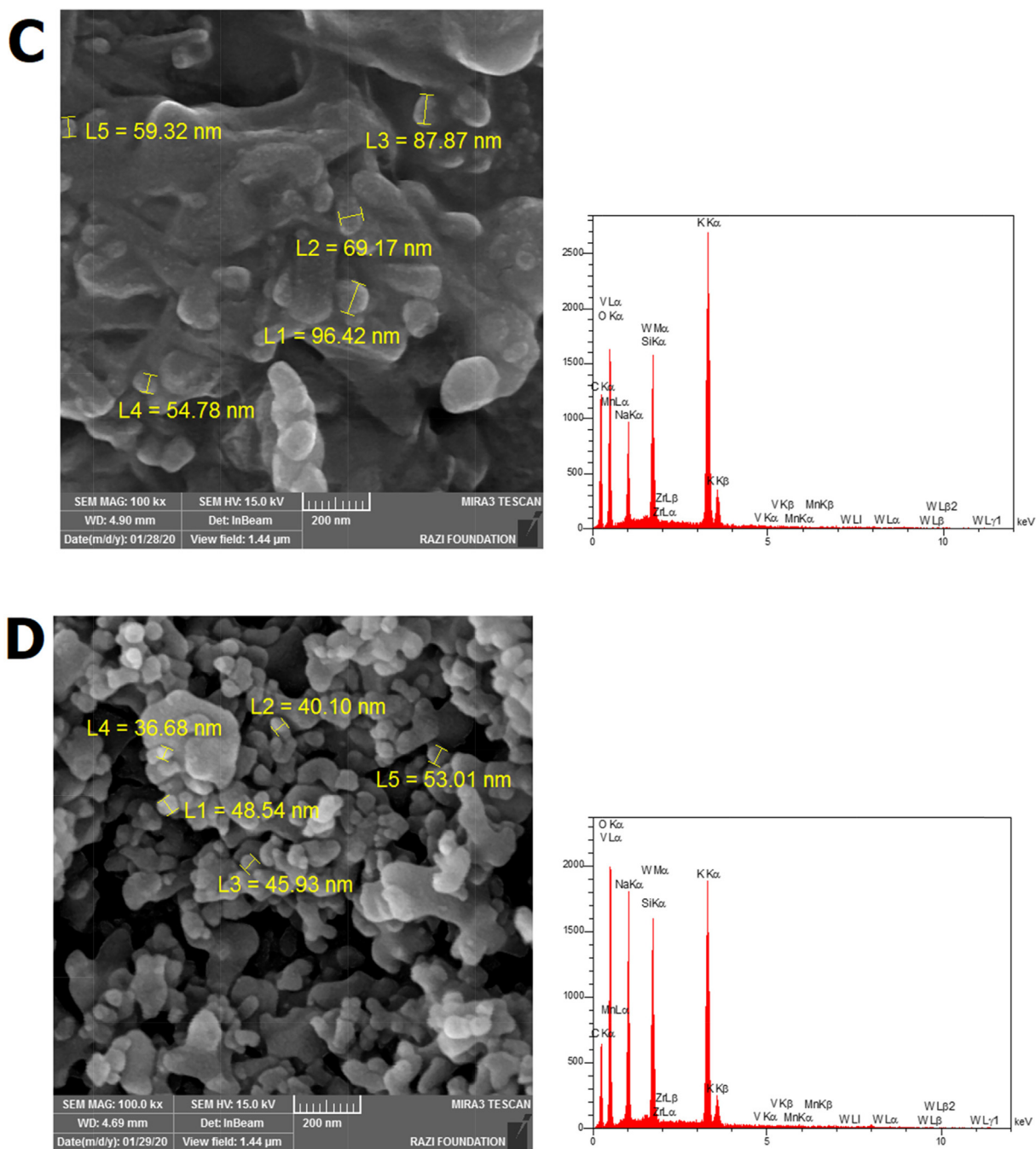


Fig. 3 (continued)

different ratio ( $\text{CH}_4/\text{O}_2 = 2, 4$  and  $6$ ) of reactants. This mixture of preheated gases was then poured onto the catalyst bed.

A mass flow controller (MFC, *Brooks Instrument*) controlled each gas flow. The mass flow controller contributed to set the nitrogen gas flow rate to a definite amount. To flow oxygen, methane and nitrogen gases in certain proportions, the reactor furnace was turned on and temperature was increased from  $775\text{ }^\circ\text{C}$  with a gradient of  $10\text{ }^\circ\text{C min}^{-1}$ . To analyze output gases from the reactor, the flame ionization detector (FID) and thermal conductivity detector (TCD) were equipped with

online gas chromatography (RGA, *Agilent 7890B, PerkinElmer*). The entire schematic design of the OCM process is presented in Fig. 1.

To study the stability of the catalyst, the test temperature was adjusted at  $850\text{ }^\circ\text{C}$  and the ratio of  $\text{CH}_4/\text{O}_2$  in the feed 2; the stability tests were performed in 50 h.

Conversion ( $\%X_{\text{CH}_4}$ ), selectivity ( $\%S_{\text{C}_2^+}$ ) and yield ( $\%Y_{\text{C}_2^+}$ ) of each catalyst were calculated according to Eq. 5–7:

$$\%X_{\text{CH}_4} = \frac{\text{moles of CH}_4 \text{ in} - \text{moles of CH}_4 \text{ out}}{\text{moles of CH}_4 \text{ in}} \times 100 \quad (5)$$

**Table 3** Reactor test results of 2% Mn – 5% Na<sub>2</sub>WO<sub>4</sub>/SiO<sub>2</sub> and NaKCO<sub>3</sub>@(Mn – Na<sub>2</sub>WO<sub>4</sub>/SiO<sub>2</sub>) (Na/K = 2/2.4) catalysts.

SCO <sub>2</sub>	S <sub>CO</sub>	Y <sub>C<sub>2</sub>H<sub>4</sub></sub>	Y <sub>C<sub>2</sub><sup>+</sup></sub>	S <sub>C<sub>2</sub><sup>+</sup></sub>	$\frac{C_2H_4}{C_2H_6}$	S <sub>C<sub>2</sub>H<sub>6</sub></sub>	S <sub>C<sub>2</sub>H<sub>4</sub></sub>	X <sub>CH<sub>4</sub></sub>	T °C	CH <sub>4</sub> /O <sub>2</sub>	Catalyst
21.79	27.99	11.02	17.07	66.78	1.82	23.68	43.10	25.56	775	2	AS-2
20.05	27.05	11.00	16.70	68.12	1.93	23.25	44.87	24.51	775	4	
18.74	29.03	10.25	15.37	66.12	2.00	22.04	44.08	23.25	775	6	
24.82	31.47	15.22	22.79	74.71	2.01	24.82	49.89	30.50	850	2	
20.58	29.70	15.10	21.72	72.74	2.28	22.18	50.56	29.86	850	4	
19.87	33.70	13.06	18.52	68.23	2.39	20.13	48.10	27.15	850	6	
4.86	6.58	15.15	21.39	66.35	2.43	19.34	47.01	32.24	775	2	CS-2
5.91	8.31	15.17	21.20	66.63	2.52	18.95	47.68	31.82	775	4	
7.67	12.58	14.07	19.59	64.10	2.55	18.06	46.05	30.55	775	6	
8.82	12.42	18.54	25.42	69.59	2.69	18.84	50.75	36.52	850	2	
11.02	14.39	18.40	24.79	70.32	2.88	18.13	52.19	35.25	850	4	
14.35	18.05	17.50	23.43	68.62	2.95	17.37	51.25	34.15	850	6	

$$\%S_{C_2^+} = \frac{\text{moles of CH}_4 \text{ that is consumed to produce C}_{2^+}}{\text{total moles of CH}_4 \text{ consumed}} \times 100 \quad (6)$$

$$\%Y_{C_2^+} = X_{CH_4} \times S_{C_2^+} \quad (7)$$

### 3. Result and discussion

#### 3.1. Catalyst characterization

The XRD test results for Mn – Na<sub>2</sub>WO<sub>4</sub>/SiO<sub>2</sub> samples show in Fig. 2, In the Mn – Na<sub>2</sub>WO<sub>4</sub>/SiO<sub>2</sub> samples,  $\alpha$ -cristobalite SiO<sub>2</sub> (JCPDS 00–003-0271) was identified to improve the catalyst activity (Almana et al., 2016). In both phase samples, Na<sub>2</sub>WO<sub>4</sub> (JCPDS 12–772) and MnO<sub>2</sub> (JCPDS 01–073-2509) were also observed (Kaviani et al., 2022).

Using Scherer equation and based on the maximum peak, the crystalline size of AS-2 and AS-3 catalyst was calculated, 28 and 48 nm, respectively. Therefore, as the Na<sub>2</sub>WO<sub>4</sub>/Mn ratio decreased from 3 to 2.5, the particle size decreased. In NaKCO<sub>3</sub>@(Mn – Na<sub>2</sub>WO<sub>4</sub>/SiO<sub>2</sub>) samples, it was found that by increasing the amount of Na and K from 0.010 and 0.012 to 0.02 and 0.024, respectively, the catalyst got a more regular structure; Also, the side phase of K<sub>2</sub>CO<sub>3</sub> (JCPDS 00–16-820) (Lee et al., 2022) was removed from the catalyst structure. The reason for the presence of this phase in the catalyst structure of CS-1 is related to the fact that some initial amount of K<sub>2</sub>CO<sub>3</sub> did not enter the shell structure, and presented in the free phase, which will reduce the efficiency and activity of the catalyst. About the CS-2 sample, no additional peaks related to the side phases of K<sub>2</sub>CO<sub>3</sub> (JCPDS 00–16-820) or Na<sub>2</sub>CO<sub>3</sub> (JCPDS 08–0448) are observed (Ziyadi et al., 2021). In the all of samples, the peak of  $\alpha$ -cristobalite SiO<sub>2</sub> was observed. Using the Scherer equation (Y. Gao et al., 2022), the crystalline size calculated for the catalyst samples CS-1 and CS-2 is 60 nm and 51 nm, respectively.

The BET surface area and pore volume of all catalysts as determined by N<sub>2</sub> adsorption are presented in Table 2. CS-2 had the highest BET (89.25 m<sup>2</sup>g<sup>-1</sup>). According to the FE-SEM images for AS-2 and AS-3 as shown in Fig. 3a-b, the particle size increased with increase the Na<sub>2</sub>WO<sub>4</sub>/Mn ratio from 2.5 to 3, the homogeneity and uniformity of the particles decreased, and the particles size of AS-3 sample was reported

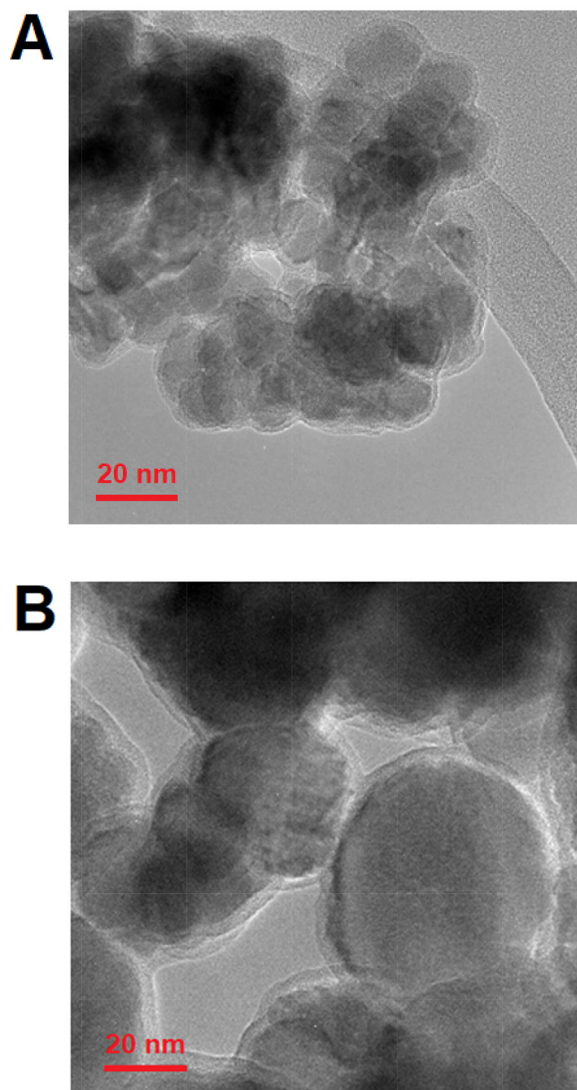
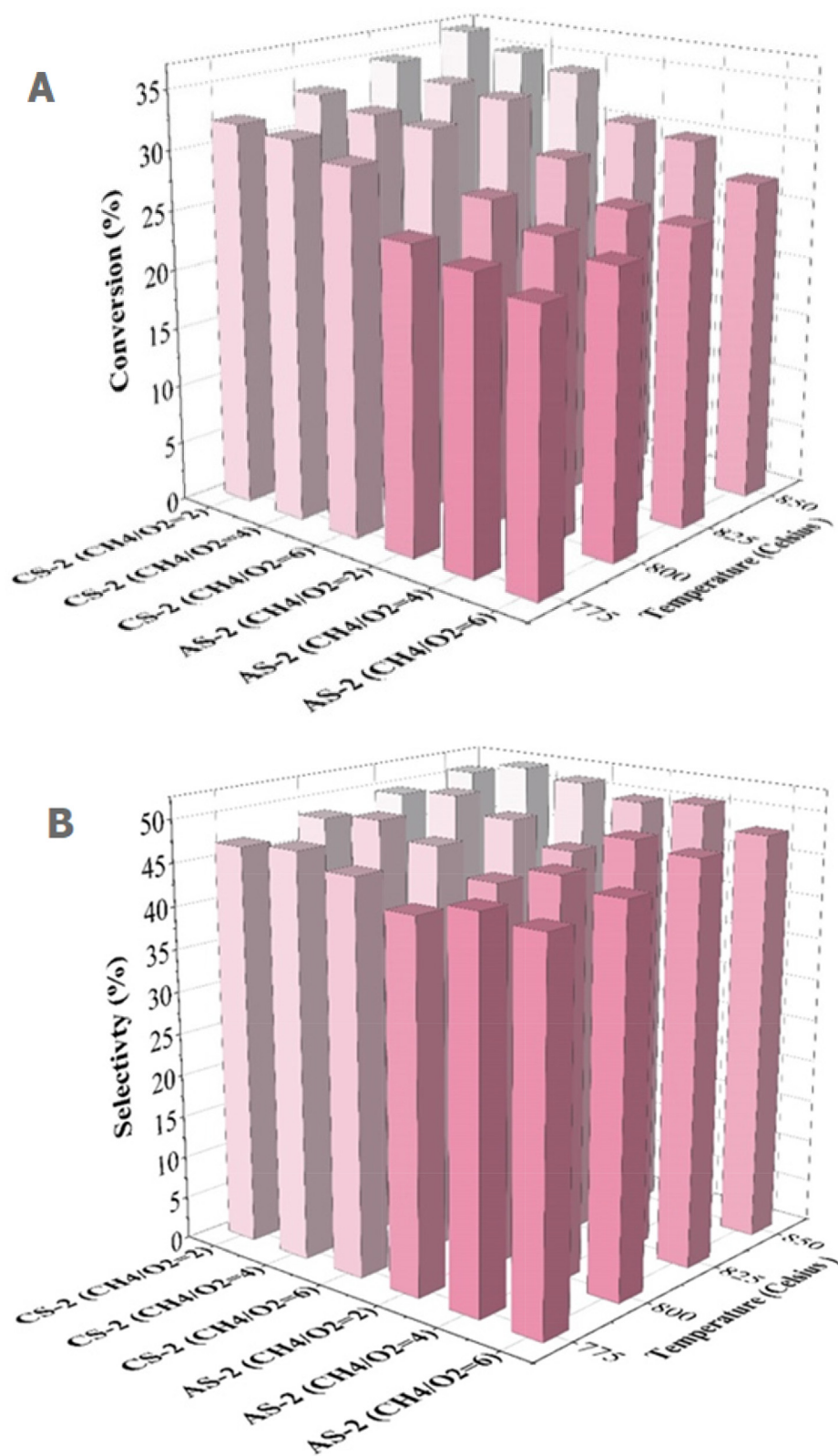


Fig. 4 TEM images for samples AS-2 (a) and CS-2 (d).

to be larger and more heterogeneous, the particle size of the AS-2 sample was observed from 29 to 48 nm and with increasing the Na<sub>2</sub>WO<sub>4</sub>/Mn ratio from 2.5 to 3, the particle size in



**Fig. 5** Methane conversion (a), selectivity (b) and  $C_2^+$  yield (c) curves in performance of AS-2 and CS-2 catalyst.

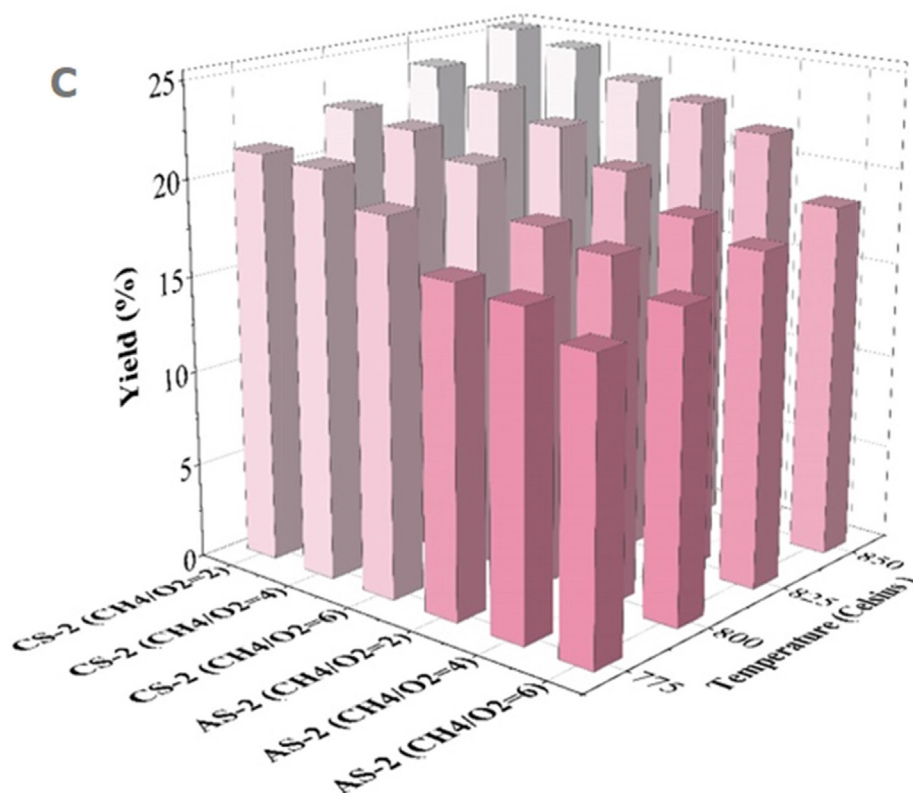


Fig. 5 (continued)

AS-3 catalyst varied between 30 and 56 nm. According to Fig. 3c-d, the core-shell samples CS-1 and CS-2, it is found that the catalyst structure becomes more regular, and the growth of the catalyst core-shell structure is increased with increasing Na and K. According to the FE-SEM analysis, the catalysts are amorphous, but according to the TEM images, it can be concluded that the catalysts are almost like spheres. Also, the size of the molecules is reduced due to the growth of the molecular network because of the improvement in the core-shell structure. The first sample, CS-1, contains 0.012 of K and 0.01 of Na had a particle with a size in the range of 54 to 96 nm and the second sample, CS-2, contains 0.024 of K and 0.02 of Na had a particle in the range of 41 to 71 nm, which is the reason for this decrease in size and is related to the growth of the core-shell structure network using increasing values of K and Na. The images related to the EDX analysis of the samples also reveal the absence of impurities in the structure of the catalysts. According to Fig. 4, the TEM image results show that the core-shell structure is formed.

According to Fig. 7, for the two catalysts CS-2 and AS-2, it is determined that the amount of carbon deposition is 0.71 % and 0.81 %, respectively, which shows the high resistance of these two catalysts against carbon sediment. The catalyst has lesser carbon sediment on its structure, which can be attributed to the presence of oxygen on its surface structure. The oxygen prevents the formation and deposition of carbon on it in the sense that by separating methane, the carbon reacts immediately with oxygen and reduces the amount of carbon deposition on the catalyst. However, it increases the amounts of

CO and  $\text{CO}_2$  as by-products. Less carbon deposition on the core-shell catalyst than a conventional AS-2 catalyst indicates better resistance of the core-shell structure because of the higher oxygen content in the CS-2 which thus increases catalyst activity and makes it more stable.

### 3.2. Catalyst activity

The results of the  $\text{Mn-Na}_2\text{WO}_4/\text{SiO}_2$  and  $\text{NaKCO}_3@(\text{Mn-Na}_2\text{WO}_4/\text{SiO}_2)$  catalyst activity test with different ratios of Mn and  $\text{Na}_2\text{WO}_4$  are presented in Table 3. The effect of the methane/oxygen ratio on conversion, selectivity, and yield are shown in Table 2, these experiments were performed inside the reactor. According to Table 2, as the ratio of methane to oxygen increases, the percentage of conversion decreases; The highest conversion percentage related to the ratio of methane/oxygen = 2 was reported. However, the selectivity of ethylene alone had an increase-decrease trend and the highest percentage of selectivity was recorded in the ratio of methane/oxygen equal to 4. Since achieving the highest conversion with the highest yield of  $\text{C}_2^+$  was the goal of optimization, the ratio of methane/oxygen = 2 was chosen (Nematollahi and Neyts, 2020).

Oxygen concentration is considered one of the main variables controlling the progress of reactions. The results showed that in the presence of oxygen, the formed  $\text{C}_2^+$  hydrocarbons can be easily converted into  $\text{CO}_x$ . By increasing the oxygen concentration in the feed gas and producing  $\text{CO}_x$ , methane was consumed at a higher rate through oxidation reactions

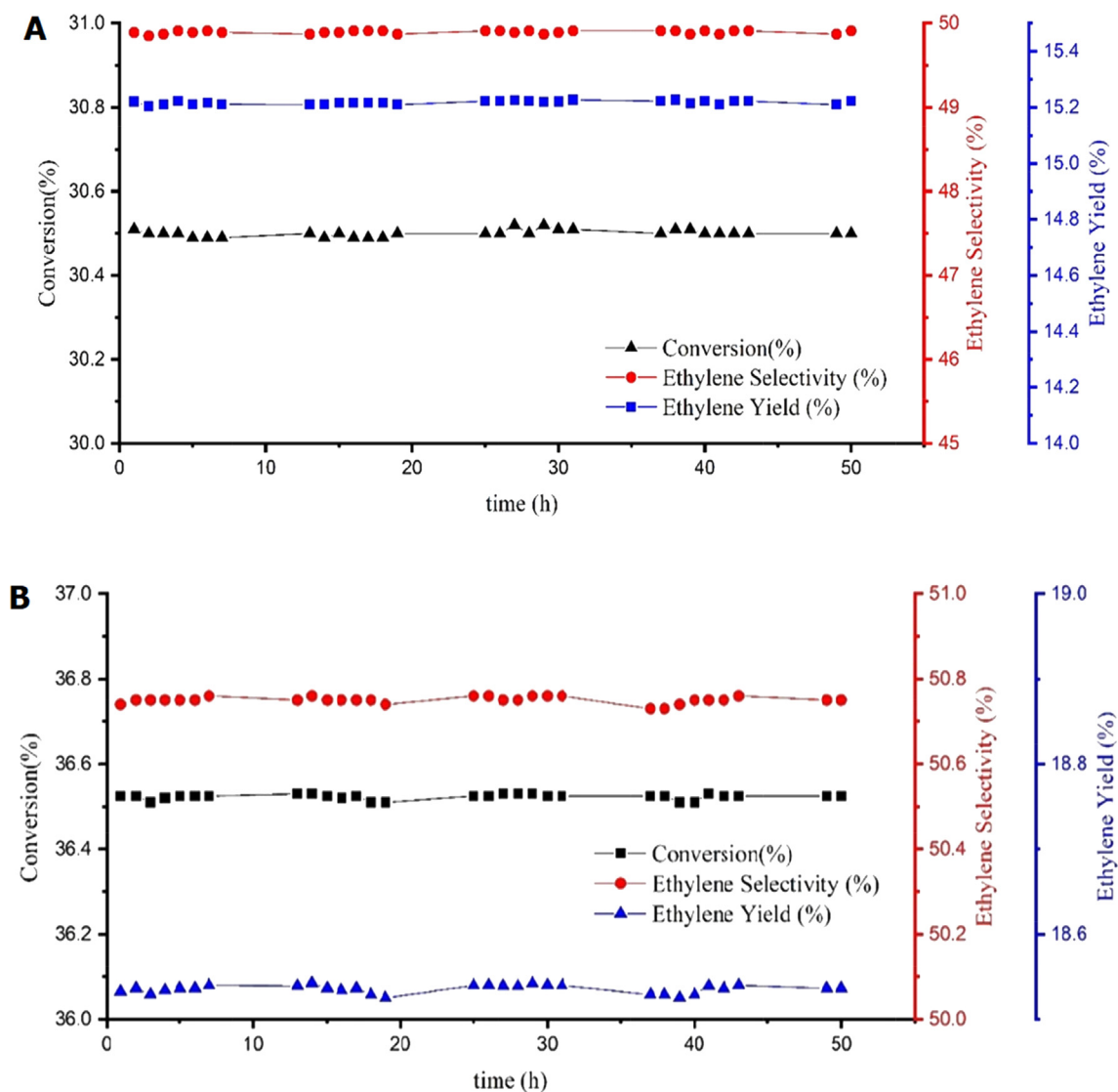


**Fig. 6** Conversion, ethylene selectivity, and ethylene yield for AS-2 (a) and CS-2 (b) catalyst over 50 h with feed containing methane, oxygen, and nitrogen at a ratio of 2:1:7 at 850 °C.

(Fig. 5a). The yield of  $C_2^+$  is the product of methane conversion percentage and the selectivity of  $C_2^+$  (Fig. 5c). Therefore, the efficacy of  $C_2^+$  decreases as the molar ratio of methane to oxygen increases. If the amount of oxygen in the feed gas is reduced, the  $CO_x$  production rate will always be lower than the  $C_2$  production rate. Therefore, as the methane to oxygen ratio increases from 2 to 6, methane conversion reduces, while the selectivity of  $C_2^+$  enhances (Fig. 5b). Therefore, higher methane conversion and  $C_2$  yield was obtained with a higher oxygen ratio (lower  $CH_4/O_2$  ratio), and the hydrocarbons in the process are oxidized less to carbon dioxide for a  $CH_4/O_2$  feed ratio (less than 2) (Liu et al., 2022).

According to Fig. 5, the reactor tests for nano-catalytic activity suggest the reactor temperature range of 775–850 °C, the methane conversion, selectivity, and yield of  $C_2$  compounds have presented the highest results. The optimum temperature was 850 °C. Methane conversion was insignificantly affected at high  $CH_4/O_2$  feed ratios for temperatures above

850 °C. The selectivity and the yield of  $C_2$  compounds at the reactor output were enhanced by increasing the reaction temperature to 850 °C.

At both temperatures, below 775 °C and above 850 °C, the gas phase reaction controls the OCM reactions. Selectivity and performance both benefit from successive reactions resulting from the gas phase reaction and reach their highest values. Above 850 °C the oxidation of  $C_2$  compounds was the main reaction causing low ethylene selectivity. As a result,  $C_2$  product performance was diminished. Maximum performance for the catalytic activity was achieved when the whole oxygen in the reactor was consumed (Rosli et al., 2022). The best performance for these two families of catalysts in similar operating conditions is mentioned below:

I) AS-2 catalyst in the feed ratio  $CH_4/O_2 = 2$  and temperature of 850 °C resulting in methane conversion percentage of 30.5 % and  $C_2$  yield of 22.79 %, selectivity of 74.71 % for  $C_2^+$  and selectivity of 49.89 % for ethylene.

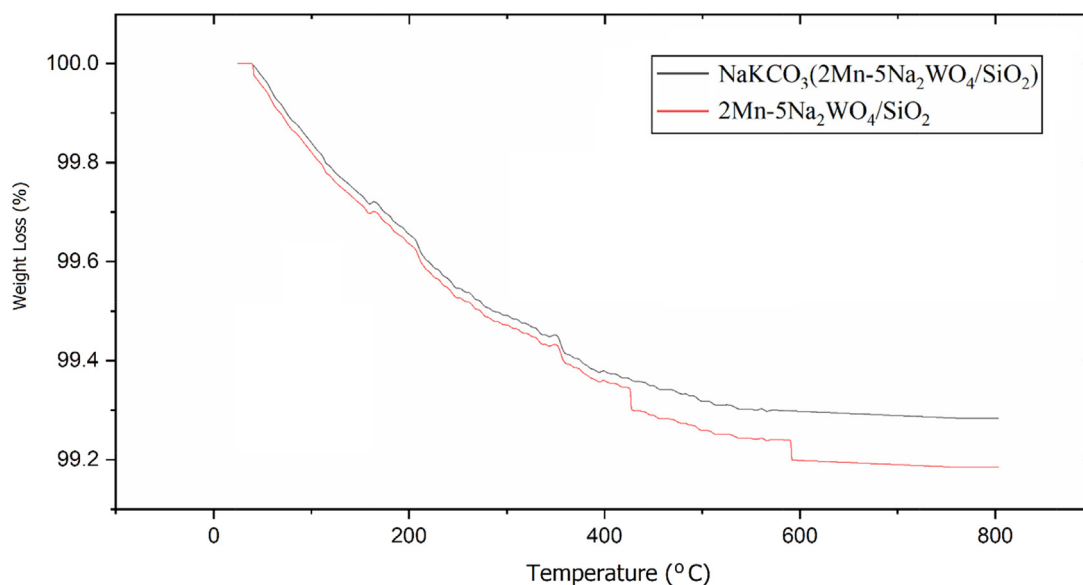


Fig. 7 TGA test results for AS-2 and CS-2 catalysts.

II) CS-2 which in the same operating conditions results in, the percentage of methane conversion of 36.52 %,  $\text{C}_2$  yield of 25.42 %, selectivity of 69.59 % for  $\text{C}_2^+$ , and selectivity of 50.75 % for ethylene.

Another distinguishing result was the difference in the amount of ethane produced as one of the by-products, which for the core-shell catalyst was lesser than the conventional AS-2 catalyst. Ethane reduces the selectivity and yield of the  $\text{C}_2$  product for the core-shell catalyst.

The ethylene produced by the core-shell catalyst was about 21 % more in comparison with the amount of ethylene produced by the conventional catalyst. And the ethane produced as a by-product was approximately 10 % lower for the core-shell catalyst resulting in a higher ratio of ethylene to ethane that was produced (Yang et al., 2022).

Regarding the AS-2 catalyst as well as its core-shell catalyst, it can be noted that the higher activity of these two catalysts in comparison with other catalysts can be related to the proper distribution of  $\text{Na}_2\text{WO}_4$  on the catalyst structure. The active phase of these catalysts consists of quadrilateral  $\text{WO}_4^{2-}$ . This structure was changed during the catalytic cycle between  $\text{W}^{6+}$  and  $\text{W}^{5+/4+}$  structures during the chemical separation of methane and subsequent methane oxidation. The main role of Na in the catalyst was to stabilize the  $\text{WO}_4^-$  quadrilateral structure versus the octahedral structure. The Mn in  $\text{Mn}_2\text{O}_3$  was a mediator that contributes to the use of the oxygen produced in the recovery of  $\text{W}^{6+}$ . The cooperation of two cycles of reduction of W and Mn leads to the development of OCM. The second role of sodium in the structure of this catalyst was to facilitate the formation of the cristobalite phase at low temperatures such as 800 °C, which was lower than the calcination temperature of  $\text{SiO}_2$ . The presence of the cristobalite phase in  $\text{SiO}_2$  stabilizes  $\text{WO}_4^-$ , sodium plays a dual role as a chemical and structural enhancer (Park et al., 2020).

One of the concerns is that at high temperatures of the OCM process, the core-shell structure breaks down to form a composite mixture composed of MnO,  $\text{NaKCO}_3$ ,  $\text{Na}_2\text{WO}_4$ ,

and  $\text{SiO}_2$ . In this research, a solution was found to solve this problem; the presence of excess sodium in the nano-catalytic structure of  $\text{NaKCO}_3$  caused a very good distribution of  $\text{Na}_2\text{WO}_4$  on  $\text{SiO}_2$  containing Mn. This proper distribution makes it easy to form  $\text{WO}_4^-$ . This prevents  $\text{WO}_4^-$  from being converted to  $\text{W}^{6+}$  due to the high amount of sodium and oxygen in the system, and improves the performance of the core-shell catalyst in comparison with a conventional catalyst. Therefore, the core-shell structure and the proper distribution of the  $\text{Na}_2\text{WO}_4$  phase in its structure improve the performance of the catalyst in the production of  $\text{C}_2$  compounds (Zhou et al., 2021).

Based on the results of the tests and the comparison of the data obtained from the conversion percentage and the yield of ethylene production, the best performance is related to the two catalysts AS-2 and CS-2. So, a stability test at 850 °C for 50 h with a feed-to-oxygen ratio of 2 was performed on these two catalysts to test their stability in addition to being superior in yield and selectivity. The results of the stability test indicated that both catalysts have high stability in ethylene production (Fig. 6).

#### 4. Conclusion

The purpose of the core-shell catalyst synthesis is to maintain the stability of the Mn –  $\text{Na}_2\text{WO}_4/\text{SiO}_2$  catalyst as the core is coated by the  $\text{NaKCO}_3$  shell to withstand the high heat of reaction. Shells protected at high reaction temperatures for longer periods improve catalytic activity. In the current research, core-shell structures composed of  $\text{Na}_2\text{WO}_4$  – Mn –  $\text{SiO}_4$  were prepared as precursors of OCM catalysts. The aim of this paper was to investigate the proper conditions for higher performance of the Mn –  $\text{Na}_2\text{WO}_4/\text{SiO}_4$  catalyst with and without  $\text{NaKCO}_3$  shell, in terms of the selectivity and yield of  $\text{C}_2^+$  and in terms of catalyst stability for a longer period. The advantage of the  $\text{NaKCO}_3$  shell is its high thermal resistance since it has no decomposition, no interference in the process, and less carbon deposition. The core-shell catalyst is more stable, and its activity loss and degradation occur later. The core-shell catalyst limits ethylene reabsorption and does not allow it to react with unsaturated cations. In

addition to increasing the yield and selectivity of ethylene as the main product, it reduces ethane production as one of the by-products. The advantage of the NaKCO<sub>3</sub> core-shell catalyst is that it is cheap and readily available. The production of other by-products in the core-shell catalyst is much lower compared to other catalysts, and this reduces the cost of separation of by-products thereby improving the performance of the catalyst in the production of the main ethylene product. In conclusion, the CS-2 core-shell catalyst has a stable methane conversion of about 36.52 % and an ethylene yield of about 18.54 %, and a C<sub>2</sub><sup>+</sup> yield of about 25.42 % at 850 °C with a CH<sub>4</sub>/O<sub>2</sub> ratio of 2, which for other catalysts are around 30.50 %, 15.22 %, and 22.79 %, respectively.

### Declaration of Competing Interest

The authors declare that they have no known competing financial interests or personal relationships that could have appeared to influence the work reported in this paper.

### Acknowledgements

This research was supported by Bandar Imam Petrochemical Company (0861638903).

### References

- Alli, R.D., de Souza, P.A.L., Mohamedali, M., Virla, L.D., Mahinpey, N., 2022. Tri-reforming of methane for syngas production using Ni catalysts: current status and future outlook. *Catal. Today*. <https://doi.org/10.1016/j.cattod.2022.02.006>.
- Almana, N., Phivilay, S.P., Laveille, P., Hedhili, M.N., Fornasiero, P., Takanabe, K., Basset, J.M., 2016. Design of a core-shell Pt-SiO<sub>2</sub> catalyst in a reverse microemulsion system: distinctive kinetics on CO oxidation at low temperature. *J. Catal.* 340, 368–375. <https://doi.org/10.1016/j.jcat.2016.06.002>.
- Gao, X., Wang, Z., Huang, Q., Jiang, M., Askari, S., Dewangan, N., Kawi, S., 2022. State-of-art modifications of heterogeneous catalysts for CO<sub>2</sub> methanation – active sites, surface basicity and oxygen defects. *Catal. Today* 402, 88–103. <https://doi.org/10.1016/j.cattod.2022.03.017>.
- Gao, Y., Wei, Y., Sun, W., Zhao, G., Liu, Y., Lu, Y., 2022. Insight into deactivation of the carbon-/sintering-resistant Ni@Silicalite-1 for catalytic partial oxidation of methane to syngas. *Fuel* 320, <https://doi.org/10.1016/j.fuel.2022.123892> 123892.
- Gärtner, C.A., Van Veen, A.C., Lercher, J.A., 2014. Oxidative dehydrogenation of ethane on dynamically rearranging supported chloride catalysts. *J. Am. Chem. Soc.* 136, 12691–12701. <https://doi.org/10.1021/ja505411s>.
- Jafarzadeh, F., Dolatkah, Z., Molaei, S., Javanshir, S., 2022. CS@Cu<sub>2</sub>O and magnetic Fe<sub>3</sub>O<sub>4</sub>@SiO<sub>2</sub>-pAMBA-CS-Cu<sub>2</sub>O as heterogeneous catalysts for CuAAC click reaction. *Arab. J. Chem.* 15. <https://doi.org/10.1016/j.arabjc.2022.103838>.
- Jaroenpanon, K., Tiyyatha, W., Chuokeaw, T., Sringam, S., Witoon, T., Wattanakit, C., Chareonpanich, M., Faungnawakij, K., Seubsai, A., 2022. Synthesis of Na<sub>2</sub>WO<sub>4</sub>-MnxOy supported on SiO<sub>2</sub> or La<sub>2</sub>O<sub>3</sub> as fiber catalysts by electrospinning for oxidative coupling of methane: synthesis of Na<sub>2</sub>WO<sub>4</sub>-MnxOy supported on SiO<sub>2</sub> or La<sub>2</sub>O<sub>3</sub> as fiber catalysts. *Arab. J. Chem.* 15. <https://doi.org/10.1016/j.arabjc.2021.103577>.
- Kaviani, M., Rezaei, M., Mehdi Alavi, S., Akbari, E., 2022. High coke resistance Ni-SiO<sub>2</sub>@SiO<sub>2</sub> core-shell catalyst for biogas dry reforming: effects of Ni loading and calcination temperature. *Fuel* 330, <https://doi.org/10.1016/j.fuel.2022.125609> 125609.
- Lee, E.J., Seo, Y., Park, H., Kim, M.J., Yoon, D., Choung, J.W., Kim, C.H., Choi, J., Lee, K.Y., 2022. Development of etched SiO<sub>2</sub>@Pt@ZrO<sub>2</sub> core-shell catalyst for CO and C<sub>3</sub>H<sub>6</sub> oxidation at low temperature. *Appl. Surf. Sci.* 575. <https://doi.org/10.1016/j.apsusc.2021.151582>.
- Liu, J., Yue, J., Lv, M., Wang, F., Cui, Y., Zhang, Z., Xu, G., 2022. From fundamentals to chemical engineering on oxidative coupling of methane for ethylene production: a review. *Carbon Resour. Convers.* 5, 1–14. <https://doi.org/10.1016/j.crcon.2021.11.001>.
- Lyu, J.M., Yu, S., Peng, Z., Zhou, J., Liu, Z., Li, X.Y., Yu-Li, Chen, L.H., Su, B.L., 2022. Control of the proximity of bifunctional zeolite@Al<sub>2</sub>O<sub>3</sub> catalysts for efficient methanol conversion into hydrocarbons. *Catal. Today*. <https://doi.org/10.1016/j.cattod.2022.07.017>.
- Nematollahi, P., Neyts, E.C., 2020. Direct oxidation of methane to methanol on Co embedded N-doped graphene: comparing the role of N<sub>2</sub>O and O<sub>2</sub> as oxidants. *Appl. Catal. A Gen.* 602, <https://doi.org/10.1016/j.apcata.2020.117716> 117716.
- Orooji, Y., Han, N., Nezafat, Z., Shafei, N., Shen, Z., Nasrollahzadeh, M., Karimi-Maleh, H., Luque, R., Bokhari, A., Klemeš, J.J., 2022. Valorisation of nuts biowaste: prospects in sustainable bio(nano)catalysts and environmental applications. *J. Clean. Prod.* 347. <https://doi.org/10.1016/j.jclepro.2022.131220>.
- Ortiz-Bravo, C.A., Chagas, C.A., Toniolo, F.S., 2021. Oxidative coupling of methane (OCM): an overview of the challenges and opportunities for developing new technologies. *J. Nat. Gas Sci. Eng.* 96, <https://doi.org/10.1016/j.jngse.2021.104254> 104254.
- Park, L.H., Jo, Y.R., Choi, J.W., Suh, D.J., Song, K.H., Ha, J.M., 2020. SiO<sub>2</sub>@MnO: X@Na<sub>2</sub>WO<sub>4</sub>@SiO<sub>2</sub> core-shell-derived catalyst for oxidative coupling of methane. *RSC Adv.* 10, 37749–37756. <https://doi.org/10.1039/d0ra05081d>.
- Raza, J., Khoja, A.H., Anwar, M., Saleem, F., Naqvi, S.R., Liaquat, R., Hassan, M., Javaid, R., Qazi, U.Y., Lumbers, B., 2022. Methane decomposition for hydrogen production: a comprehensive review on catalyst selection and reactor systems. *Renew. Sustain. Energy Rev.* 168, <https://doi.org/10.1016/j.rser.2022.112774> 112774.
- Rosli, S.N.A., Abidin, S.Z., Osazuwa, O.U., Fan, X., Jiao, Y., 2022. The effect of oxygen mobility/vacancy on carbon gasification in nano catalytic dry reforming of methane: a review. *J. CO<sub>2</sub> Util.* 63, <https://doi.org/10.1016/j.jcou.2022.102109> 102109.
- Song, J., Ma, N., Chen, W., Chen, J., Dai, Q., 2022. Insights into mechanism of catalytic ozonation of cinnamyl alcohol over core-shell Fe<sub>3</sub>O<sub>4</sub>@SiO<sub>2</sub>@La<sub>2</sub>O<sub>3</sub> catalyst. *Sep. Purif. Technol.* 282, <https://doi.org/10.1016/j.seppur.2021.119969> 119969.
- Tiyatha, W., Chuokeaw, T., Sringam, S., Witoon, T., Chareonpanich, M., Ruppachter, G., Seubsai, A., 2022. Oxidative coupling of methane—comparisons of MnTiO<sub>3</sub>-Na<sub>2</sub>WO<sub>4</sub> and MnO<sub>x</sub>-TiO<sub>2</sub>-Na<sub>2</sub>WO<sub>4</sub> catalysts on different silica supports. *Sci. Rep.* 12, 1–16. <https://doi.org/10.1038/s41598-022-06598-6>.
- Wang, H., Zhang, J.F., Bai, Y.X., Wang, W.F., Tan, Y.S., Han, Y.Z., 2016. NiO@SiO<sub>2</sub> core-shell catalyst for low-temperature methanation of syngas in slurry reactor. *Ranliao Huaxue Xuebao/J. Fuel Chem. Technol.* 44, 548–556. [https://doi.org/10.1016/s1872-5813\(16\)30024-x](https://doi.org/10.1016/s1872-5813(16)30024-x).
- Yang, J., Wang, J., Zhao, J., Bai, Y., Du, H., Wang, Q., Jiang, B., Li, H., 2022. CO<sub>2</sub> conversion via dry reforming of methane on a core-shell Ru@SiO<sub>2</sub> catalyst. *J. CO<sub>2</sub> Util.* 57, <https://doi.org/10.1016/j.jcou.2022.101893> 101893.
- Yentekakis, I.V., Panagiotopoulou, P., Artemakis, G., 2021. A review of recent efforts to promote dry reforming of methane (DRM) to syngas production via bimetallic catalyst formulations. *Appl. Catal. B Environ.* 296, <https://doi.org/10.1016/j.apcatb.2021.120210> 120210.
- Zhang, H., Sun, Z., Hu, Y.H., 2021. Steam reforming of methane: current states of catalyst design and process upgrading. *Renew. Sustain. Energy Rev.* 149, <https://doi.org/10.1016/j.rser.2021.111330> 111330.
- Zhang, H., Chen, W., Wang, H., Tong, X., Wang, Y., Yang, X., Wu, Z., Liu, Z., 2022. A core-shell NiCu@NiCuOOH 3D electrode induced by surface electrochemical reconstruction for the ammonia

- oxidation reaction. *Int. J. Hydrogen Energy* 47, 16080–16091. <https://doi.org/10.1016/j.ijhydene.2022.03.139>.
- Zhang, J., Gu, F., Wang, C.A., 2021. Facile synthesis of multi-shelled MnO<sub>2</sub>-Co<sub>3</sub>O<sub>4</sub> hollow spheres with superior catalytic activity for CO oxidation. *Ceram. Int.* 47, 18411–18416. <https://doi.org/10.1016/j.ceramint.2021.03.164>.
- Zhou, X., Pang, Y., Liu, Z., Vovk, E.I., van Bavel, A.P., Li, S., Yang, Y., 2021. Active oxygen center in oxidative coupling of methane on La<sub>2</sub>O<sub>3</sub> catalyst. *J. Energy Chem.* 60, 649–659. <https://doi.org/10.1016/j.jechem.2021.01.008>.
- Ziyadi, H., Baghali, M., Heydari, A., 2021. The synthesis and characterization of Fe<sub>2</sub>O<sub>3</sub>@SiO<sub>2</sub>-SO<sub>3</sub>H nanofibers as a novel magnetic core-shell catalyst for formamidine and formamide synthesis. *Heliyon* 7. <https://doi.org/10.1016/j.heliyon.2021.e07165>.